An Enhanced Fourier Transform Spectrometer with a Search Algorithm

Shiunn-Jang Chern and Kuo-Jiann Chao

Abstract—**Interferometric instruments have the following serious weak points: 1) the necessity of doing a Fourier transform that involves a vast amount of calculation; 2) the lack of knowledge of suitable measuring conditions until the Fourier transform is finished; and 3) the spectral resolution of the conventional Fourier-based techniques is significantly affected by the sampling rate, data length, and noise in signal processing. In this paper, an enhanced spectrometer is proposed using the modified forward-backward linear prediction method (MFBLP) with a search algorithm. To document the advantage of the method presented, a computer simulation for multiple-wavenumber estimation is investigated. The MFBLP method is truly superior to the fast Fourier transform (FFT) method. In general, the spectral resolution using the FFT method is proportional to the data length. In this paper, however, we will show that excellent results can also be obtained from only 60 sample points using the FFT method. Moreover, from experimental results, we also conclude that the sampling rate must be consistent with the condition $632 < f_p \cdot t \cdot D < 3164$, where f_p represents the value of the pulse generator frequency in Hz, t the observation time, and D the decimation factor.**

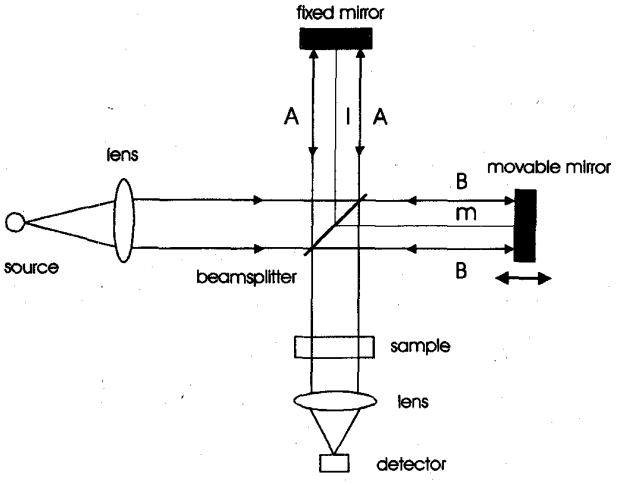

Fig. 1. Basic Michelson interferometer optical diagram.

I. Introduction

It is well known that an important feature of interferometric (e.g., the Michelson-type) spectrometers is that they allow a fast optical system to have the Fellgett advantage; i.e., the ability to measure radiation from the entire spectral region passing through the system at all times. This feature is especially effective for obtaining far IR spectra. The applications of Fourier transform spectroscopy or interferometry in science and industry are extensive. The usefulness and simplicity of this technique lend it to use in almost every field into which the spectroscopist has ventured and into some where he has not yet gone. Fourier transform spectroscopy has an advantage in most instances over conventional techniques, but interferometric instruments have the following serious weak points: 1) the necessity of doing Fourier transformations that involve a vast amount of calculation; 2) the lack of knowledge of suitable measuring conditions until the Fourier transform is finished; and 3) the spectral resolution of the conventional Fourier-based techniques is significantly affected by the data length, decimation factor, and noise in signal processing. In this paper, we propose a spectrum estimation method referred to as the modified forward and backward linear prediction method with a search algorithm, or in short, the search algorithm, for optical spectroscopy analysis. Experimental results will demonstrate that the method presented retains the advantages of interferometric instruments and overcomes their weak points.

Manuscript received June 15, 1993; revised March 2, 1995. This work was supported by the National Science Council, Republic of China, under Contract NSC-80-0404-E-110-17.

The authors are with the Department of Electrical Engineering, National Sun Yat-Sen University, Kaohsiung, Taiwan 80424, R.O.C.

Publisher Item Identifier S 0018-9456(96)00072-1.

II. Methods of Analysis

A. The Principle of the Spectrometer

A Fourier transform spectrometer (FTS) is essentially a modified Michelson interferometer [1], [2]. Fig. 1 is an optical diagram of the basic Michelson interferometer; it consists of two mirrors, M_1 and M_2, and a beamsplitter at 45° with respect to their normals. After the radiation beam is collimated by a lens, its amplitude is divided by the beamsplitter. One part of the radiation beam, A, reflected from the beamsplitter, goes to and returns from a fixed mirror, and then is transmitted through the beamsplitter. The other part of the radiation beam, B, goes through the beamsplitter to a movable mirror, which reflects the beam back. The beam, B, is reflected from the beamsplitter and mixed with beam A. The resultant beam passing through a sample area is then collected by a focusing lens and directed to a detector. When the distance m as shown in Fig. 1 is not equal to the l, the difference of these two paths is defined as the optical path difference (OPD), $\delta = 2(m - l)$. In this case, the combined beams will produce interference arising from a phase difference. Consequently, the interferogram is an intensity variation pattern corresponding to phase difference.

Now, assuming perfect optics and considering an incident monochromatic wave with amplitude $4E_0(\sigma)$, where σ is the wavenumber, $\sigma = \frac{1}{\lambda}$, and is measured in μm^{-1}, the amplitude reflected from the fixed mirror and passed to the detector can thus be presented as

$$y_1(z) = E_0(\sigma)e^{j2\pi z/\lambda} \tag{1}$$

and the amplitude reflected by the movable mirror and reflected to the detector is

$$y_2(z) = E_0(\sigma)e^{j2\pi(z+\delta)/\lambda}. \tag{2}$$

Using the law of superposition, one finds the recombining amplitude as $A = y_1(z) + y_2(z)$. Therefore, the signal received by the detector is a variation of intensity, i.e.,

$$\begin{aligned} I(\delta) \propto |A|^2 &= A^*A \\ &= 2E_0^2(\sigma)(1+\cos(2\pi\delta/\lambda)). \end{aligned} \tag{3}$$

When the movable mirror displacement occurs with constant speed, v, for t s, $\delta = 2vt$; hence, from (3) we have

$$2\pi\delta/\lambda = 2\pi(2v/\lambda)t. \tag{4}$$

Consequently, the frequency of the interferogram is, for a given wavelength λ,

$$f = 2v/\lambda = 2v\sigma. \tag{5}$$

This frequency, f, can be calculated by taking a Fourier transform of the sampled interference pattern. If the velocity, v, of the movable mirror is known, the wavelength or wavenumber can be determined from (5) [3].

The variational part of the intensity of a nonmonochromatic wave, which consists of a group of cosine waves with different frequencies, can be written as

$$I(\delta) = \sum_{i=1}^{\infty} B(\sigma_i)\cos(2\pi\delta\sigma_i) \tag{6}$$

where $B(\sigma_i)$ is a discrete spectrum corresponding to σ_i. If the light source has a continuous spectrum, then we can replace the summation by an integral in (6). For convenience, the cosine function will be presented in exponential form as

$$\text{Interferogram} \qquad I(\delta) = \int_{-\infty}^{\infty} B(\sigma)e^{j2\pi\delta\sigma}d\sigma. \tag{7}$$

Equation (7) describes the interference pattern. By taking the Fourier transform of (7), we can get the corresponding spectrum

$$\text{Spectrum} \qquad B(\sigma) = \int_{-\infty}^{\infty} I(\delta)e^{-j2\pi\delta\sigma}d\delta. \tag{8}$$

We have referred to (7) and (8) as the Fourier transform pair. If high resolution is desired in (8), the displacement of the mirror must be increased appropriately. However, the mirror displacement is finite. In fact, the resolution is also influenced somewhat by processing (windowing). The maximum displacement of OPD is denoted by $\Delta = \delta_{\max}$, which determines the resolution of the interferometer, $\Delta_\sigma = \frac{1}{\Delta}\ \mu\text{m}^{-1}$. Fortunately, the previous hardware limitation can be easily improved by using a signal-processing technique.

B. Modified Forward-Backward Linear Prediction Method (MFBLP)

The modified forward-backward linear prediction method (MFBLP) was proposed by Tufts and Kumaresan [4]. They used the eigen-decomposition method to approximate the least square solution in the FBLP method. For convenience in discussing the MFBLP method, we first use Figs. 2 and 3 to introduce the so-called forward-backward linear prediction (FBLP) method. Fig. 2 shows a forward prediction error filter with L tap weights, $g_1, g_2, \cdots, g_L$, and L tap inputs that are drawn from a tap delay line, respectively. The operation of the prediction may involve using the present signal to make an estimation of a future signal. Furthermore, we adapt the tap weight coefficients to optimize the mean square error [5]. Conversely, the backward prediction error filter, which is shown as Fig. 3, uses the past values to make an estimation of the present signal. Their tap weight coefficients compared with those of the forward prediction error filter have the reverse order and the complex conjugate relationships. Assume that the detected signal is

$$\begin{aligned} y(n) &= \sum_{i=1}^{M} A_i e^{j(2\pi f_i n+\psi_i)} + w(n) \\ &\text{for} \quad n = 0, 1, \cdots, N-1 \end{aligned} \tag{9}$$

which consists of M narrow-band signals and white Gaussian noise, $w(n)$. Also, in (9), ψ_i represents the phase of the ith narrow-band signal and is assumed to be uniformly distributed over [0,2π) to preserve wide-sense stationarity. Then, using the prediction filter on the N data samples, we can write the prediction equation in a matrix form as

$$\begin{aligned} &\begin{bmatrix} y(L) & y(L-1) & \cdots & y(1) \\ y(L+1) & y(L) & \cdots & y(2) \\ \vdots & \vdots & \ddots & \vdots \\ y(N-1) & y(N-2) & \cdots & y(N-L) \\ y^*(2) & y^*(3) & \cdots & y^*(L+1) \\ y^*(3) & y^*(4) & \cdots & y^*(L+2) \\ \vdots & \vdots & \ddots & \vdots \\ y^*(N-L+1) & y^*(N-L+2) & \cdots & y^*(N) \end{bmatrix} \begin{bmatrix} g_1 \\ g_2 \\ \vdots \\ g_L \end{bmatrix} \\ &= -\begin{bmatrix} y(L+1) \\ y(L+2) \\ \vdots \\ y(N) \\ y^*(1) \\ y^*(2) \\ \vdots \\ y^*(N-L) \end{bmatrix} \end{aligned} \tag{10}$$

where $(\cdot)^*$ represents the complex conjugate. Equation (10) is the so-called Yule-Walker equation and can be written in a matrix form as

$$\mathbf{A}\hat{\mathbf{g}} = -\hat{\mathbf{h}}. \tag{11}$$

Since Matrix $\mathbf{A}$ is not a square matrix, we multiply by $\mathbf{A}^{\mathbf{H}}$, where the superscript $\mathbf{H}$ is denoted as the Hermitian transpose,

on both sides of (11), to obtain

$$\tilde{\mathbf{R}}\hat{\mathbf{g}} = \hat{\mathbf{r}}. \tag{12}$$

It can be seen that (12) is the normal equation resulting from minimizing the linear predictor (LP) error [6] power, and that $\tilde{\mathbf{R}}$ is the deterministic correlation matrix. The correlation matrix, $\tilde{\mathbf{R}}$, can be expressed in terms of its eigenvalues and eigenvectors, i.e.,

$$\tilde{\mathbf{R}} = \mathbf{U}\Lambda\mathbf{U}^{\mathbf{H}} \tag{13}$$

with matrices $\mathbf{U}$ and $\mathbf{\Lambda}$ defined as

$$\mathbf{U} = [\hat{\mathbf{u}}_1, \hat{\mathbf{u}}_2, \cdots, \hat{\mathbf{u}}_L], \tag{14}$$

$$\Lambda = \text{diag}[\lambda_1, \lambda_2, \cdots, \lambda_L], \tag{15}$$

respectively. Here, the eigenvalues, λ_i, of $\tilde{\mathbf{R}}$ are arranged in the decreasing order, and $\hat{\mathbf{u}}_i$ is the corresponding eigenvector of λ_i. Whether noise is present or not, substituting (13) into (12), we can get the weight vector, $\hat{\mathbf{g}}$, which is given by

$$\hat{\mathbf{g}} = \sum_{i=1}^{L} (1/\lambda_i)\hat{\mathbf{u}}_i\, \hat{\mathbf{u}}_i^{\mathbf{H}}\, \hat{\mathbf{r}}. \tag{16}$$

If no noise is present, we have M large principal eigenvalues, and the remainders are all zero. On the other hand, the eigenvalues λ_i, $i = M+1, \cdots, L$ will not be zero in the noisy case; that is, these eigenvalues are introduced by the noise component in the received signal. This procedure is the so-called FBLP method. The main difference between the FBLP and the MFBLP methods is that the MFBLP method can be used to alleviate the undesired effects due to the eigenvectors of the noise subspace. Consequently, when the eigenvalues and corresponding eigenvectors that are produced by the noise subspace are ignored, the weight vector used in spectrum estimation is given by [4]

$$\hat{\mathbf{g}} = \sum_{i=1}^{M} (1/\lambda_i)\hat{\mathbf{u}}_i\, \hat{\mathbf{u}}_i^{\mathbf{H}}\, \hat{\mathbf{r}}. \tag{17}$$

The solution of $\hat{\mathbf{g}}$ in (17) is also referred to as the principal component approach. When tap weight coefficients are calculated, the spectrum can be obtained by substituting weights into the formula derived by Griffiths in 1975 [7] as

$$S(\omega) = \frac{1}{|H(e^{j\omega})|^2} \tag{18}$$

$$H(e^{j\omega}) = 1 + \sum_{k=1}^{L} g_k e^{-jk\omega}, \quad |\omega| \le \pi. \tag{19}$$

C. Search Algorithm

The constraint of the MFBLP method is that the number of signal sources has to be known in advance and may not be available in practical applications. Therefore, based on the information about noise power, we propose a search algorithm to automatically extract the principal eigenvalues corresponding to the different optical wavenumbers. The method of MFBLP with the search algorithm is, therefore, referred to as the search algorithm. To propose a search procedure, let us discuss the

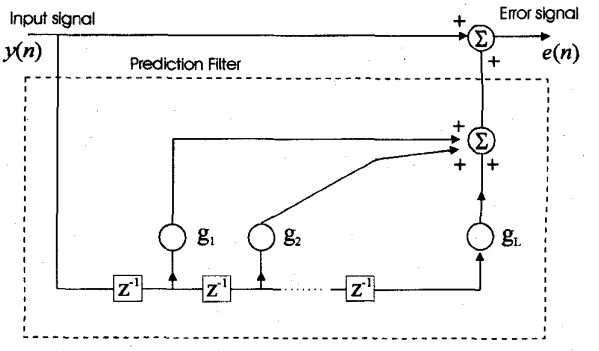

Fig. 2. Forward prediction error filter.

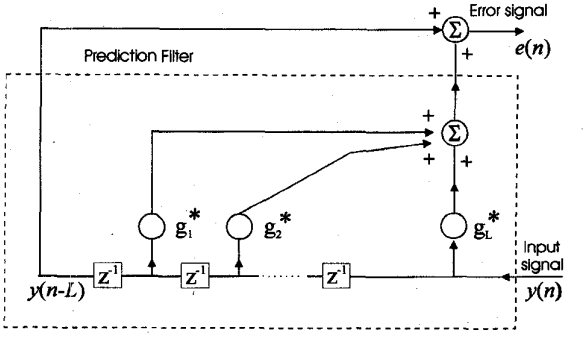

Fig. 3. Backward prediction error filter.

noise power when noise is present in the received signal. Theoretically, from (16) and (17), we see that the $(L - M)$ small eigenvalues are estimates of the noise power. Thus, if the average noise power, σ_ω^2, is available, then the following relationship will hold:

$$(L - M)\sigma_\omega^2 = \sum_{i=M+1}^{L} \lambda_i$$

$$\lambda_1 > \lambda_2 > \lambda_3 > \cdots > \lambda_L. \tag{20}$$

Based on (20), a search algorithm used to extract the principal eigenvalues is proposed and is depicted in Fig. 4. Basically, the search method, illustrated in Fig. 4, is based on the knowledge of the noise power.

To describe the procedure, some dummy variables in Fig. 4 are defined.

1) **Tpower** is the total power, can be estimated from the input signals, and is, theoretically, equivalent to the sum of all the eigenvalues.
2) **Signal** stands for the sum of the principal eigenvalues.
3) **Noise** is the noise power (the sum of eigenvalues corresponding to the noise components) and is computed by subtracting **Signal** from **Tpower**; e.g., **Tpower** − **Signal**.
4) σ_ω^2 is the average noise power estimated by the adaptive line-enhancer (ALE), depicted in Fig. 5.

As described before, σ_ω^2 can be estimated with the help of the ALE, which is depicted in Fig. 5. The ALE consists of a delay element and a linear predictor. The predictor output, $\hat{x}(n)$, is subtracted from the input signal, $x(n)$, to produce

λ_i:eigenvalue, $i = 1, 2, \cdots, L$; $\lambda_1 > \lambda_2 > \cdots > \lambda_L$

Tpower: Total power$(=\sum_{i=1}^{L} \lambda_i)$

Signal: Total signal power(the summation of the principal eigenvalues)

Noise: Total noise power(**=Tpower - Signal**)

$\hat{\sigma}_o^2$:Estimate noise variance

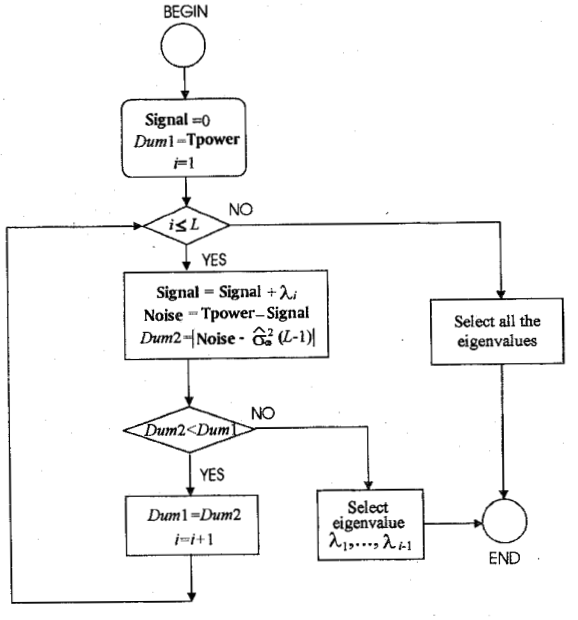

Fig. 4. Flow chart of the search procedure.

the estimation error $e(n)$. The estimation error is used to adaptively control the coefficients of the predictor, where the adaptive algorithm used here is the least mean-square (LMS) algorithm. The predictor input equals the original input signal delayed by a τ-step. The main function of the delay parameter τ is to remove the correlation that may exist between the noise component in the original input signal $x(n)$ and the noise component in the delayed predictor input $x(n-\tau)$. An ALE may, thus, be viewed as an adaptive filter that is designed to suppress broadband components (e.g., white noise) contained in the input, while at the same time passing narrowband components (e.g., sinusoid waves) with little attenuation. When the LMS algorithm has converged, the estimated error square will approach the noise variance, which is what we want. Due to the convergence property of the LMS adaptive algorithm, in general, we need more samples to achieve desired performance. Therefore, for a short data record the time-domain LMS adaptive algorithm may not be suitable for noise estimation. However, by recirculating the input data to the time-domain LMS adaptive algorithm many times, we may achieve the goal described above. The configuration of the time-domain ALE having the ability to recirculate the input data is depicted in Fig. 6 [8].

III. Results and Discussion

For convenience in describing the problem concerned with an optical signal sampled in the different cases, each set

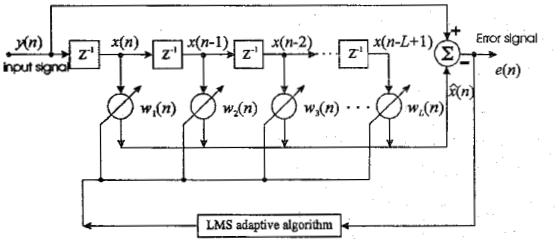

Fig. 5. Block diagram of adaptive line-enhancer (ALE).

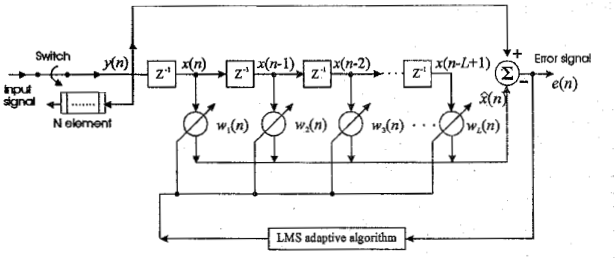

Fig. 6. Block diagram of the recirculation of the input data adaptive line-enhancer.

of sampled signals will be denoted by a remark number. In H20-4, for example, the "H" represents the He-Ne laser beam, 20 denotes the pulse frequency, and 4 (seconds) is the observation time. In this study, the length of sampled data for all signal sets is 1000 points. For the signal set H20-4, the data length is 100 points when the signal set is decimated by $D = 10$. The decimator functions by low-pass filtering the input signal and then compressing the samples [9], [10]. The procedure of optical signal processing described in this paper is depicted in Fig. 7. Also, the operation of the decimator just described is shown in Fig. 8.

The selection of the number of tap weights for the MFBLP method depends on the amount of data available. However, for wavelength estimation the greater the number of tap weights the more computation time is required. From [4] and [6], we know that the number of tap weights is proportional to the length of data points, and the empirically derived result is given by $L = \frac{3}{4}N$. But, as shown in Table IV, this is not a unique value. For convenience, we consider the tap weights to be 30, and the length of data points is chosen to be 60. This means that only 60 points from the previously decimated data (100 decimated data) are acquired. There are many ways that we can have our 60 data points from the 100 decimated data. For example, we can pick a data set in sequence from 1 to 60, or pick 2–61, 3–62, $\cdots$, 41–100, etc.

Now, for wavelength estimation, we simply apply the 60 data points to both the FFT method and the method of MFBLP with search algorithm. To give better resolution, the FFT for a data sequence with the length of 2048 is considered. For the data points being 60, we will pad zeros to fill out the sequence length to be 2048 points, so a power-of-two FFT algorithm can be employed to obtain the spectrogram of the optical signal.

To see the effect due to environmental disturbance, we consider the signal set of H20-4; here, 7 sets of optical signals of the H20-4 were obtained arbitrarily. Fig. 9 shows the best

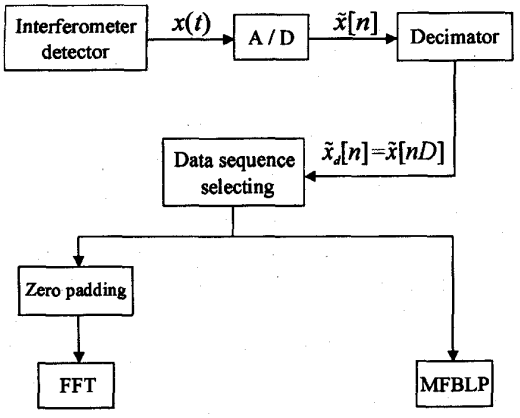

Fig. 7. Flow chart of the signal-processing procedure.

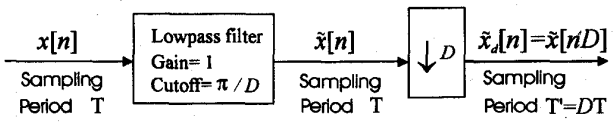

Fig. 8. General system for sampling rate reduction by D.

result among the 7 sets, because the estimated wavelength is closer to the true value 0.6328 μm. The worst result is shown in Fig. 10. It is evident from both Figs. 9 and 10 that the estimation precision was influenced by the environment during the processing of the optical signal.

Moreover, we would like to understand how the estimation results were influenced by the frequency of the pulse generator and data length in the sampling process. To do so, the optical signals H20-4 and H100-8 were examined. In the case of H100-8, since the signal variation frequency is 10 times that of the H20-4 due to the movable mirror displacement occurring at a faster speed, the decimation with $D = 10$ as in H20-4 is not required, as can be seen from Figs. 9(a) and 11(a). Therefore, for wavelength estimation, 60 data points are adopted directly from the 1000 original data points for further processing. The corresponding results using both the FFT method and the method of MFBLP with search algorithm are given in Figs. 9(b) and (c), and 11(b) and (c), respectively. We observe that all the figures estimate the wavelength as 0.6326 μm very close to the true value of 0.6328 μm, except for Figs. 9(b) and 11(b), which is the result of using the FFT method. It is important to emphasize that only 60 data points are used for wavenumber estimation by both methods. In general, we know that the spectral resolution is proportional to data length and sampling rate. In this paper, however, we found that excellent results can also be obtained from only 60 sample points. To investigate the effect due to data length with different decimation factor, three tables are listed which contain results obtained by the FFT method.

Recall that in the FFT method, 2048 points are used to obtain the spectrogram. To see the effect with different data points and decimation factor, we first consider the case with $D = 8$, that is, 125 decimated data points can be obtained, corresponding to the original signal set with 1000 data points.

TABLE I
RESULTS OF THE FFT FOR DATA LENGTH = 60, PADDED ZEROS TO 2048 AND CASE IN DECIMATION OF 8

Index	f"(1/samples)	wavenumber	wavelength
206	0.1005859	1.571655 μm^{-1}	0.6362720 μm
207	0.1010742	1.579284 μm^{-1}	0.6331980 μm
208	0.1015625	1.586914 μm^{-1}	0.6301539 μm

TABLE II
RESULTS OF THE FFT FOR DATA LENGTH = 240, PADDED ZEROS TO 2048 AND CASE IN DECIMATION OF 2

Index	f"(1/samples)	wavenumber	wavelength
51	0.02490235	1.556397 μm^{-1}	0.6425096 μm
52	0.02539063	1.586914 μm^{-1}	0.6301539 μm
53	0.02587891	1.617432 μm^{-1}	0.6182640 μm

TABLE III
RESULTS OF THE FFT FOR DATA LENGTH = 240, PADDED ZEROS TO 8192 AND CASE IN DECIMATION OF 2

Index	f"(1/samples)	wavenumber	wavelength
206	0.0251465	1.571655 μm^{-1}	0.6362720 μm
207	0.0252686	1.579284 μm^{-1}	0.6331980 μm
208	0.0253906	1.586914 μm^{-1}	0.6301539 μm

TABLE IV
OMPUTATION TIME AND THE RESULT OF WAVELENGTH ESTIMATION WITH DIFFERENT DATA LENGTH AND ORDER OF Tap–WEIGHT FOR $D = 10$

Orders	Data length	Do loop 200 times (seconds)	Average time (seconds)	Estimated results
30	50	51.48	0.2574	0.6326 μm
	40	43.56	0.2178	0.6326 μm
	35	39.60	0.198	0.6350 μm
	30	21.34	0.1067	infinity
20	50	24.75	0.12375	0.6326 μm
	40	20.79	0.10395	0.6326 μm
	35	19.8	0.099	0.6326 μm
	30	17.82	0.0891	0.6302 μm
10	50	10.89	0.05445	0.6326 μm
	40	8.82	0.0441	0.6326 μm
	30	6.79	0.03395	0.6302 μm
	20	4.85	0.02425	0.6253 μm
	10	4.85	0.02425	infinity

Again, 60 data points are adopted from the 125 decimated data points and applied to the FFT method. For 60 data points, clearly, we have fairly good results, the estimated wavelength being 0.6331980 μm, as shown in Table I. Here, the index 207, in Table I, means that the estimated value is located at the 207th scale on the frequency axis.

On the other hand, for 1000 original data points with decimation factor $D = 2$, we will have 500 decimated data points. Similarly, 240 data points are adopted from the 500 decimated data points for wavelength estimation. To obtain the spectrogram for wavelength estimation, the FFT algorithm with 2048 points is employed as in the case shown in Table I. From the frequency conversion, we can observe that the main lobe of the spectrogram is at index 52 of the FFT bin, as shown in Table II. To enhance the spectral resolution of Table II, the data length for the FFT algorithm is quadrupled, that

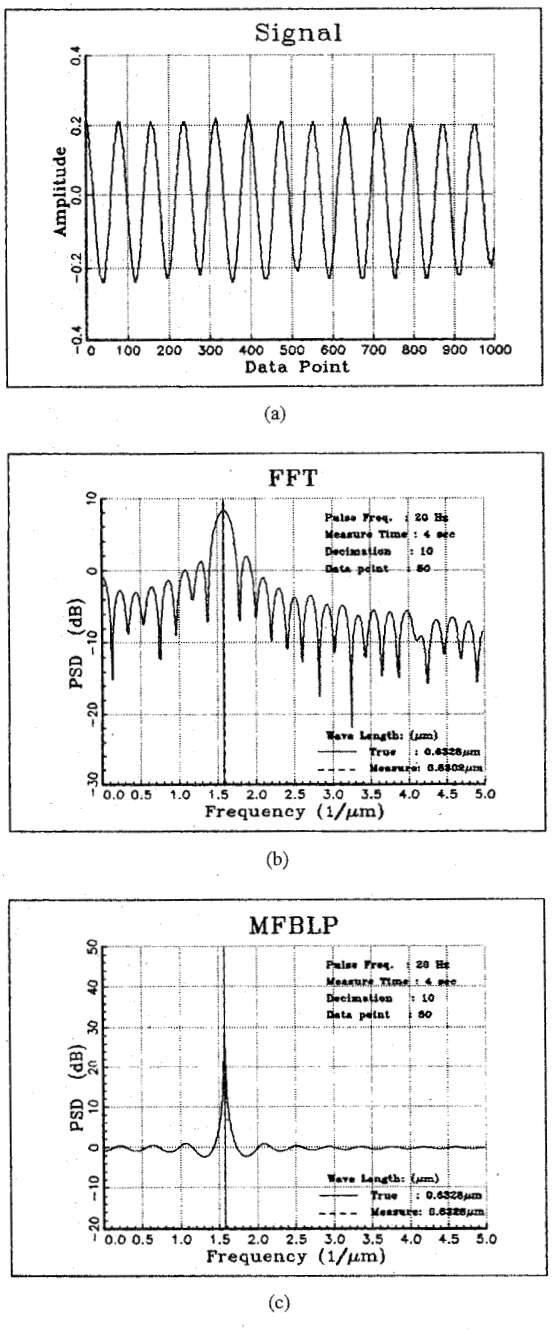

Fig. 9. (a) Waveform of the best H20-4. (b) FFT of the best H20-4. (c) MFBLP of the best H20-4.

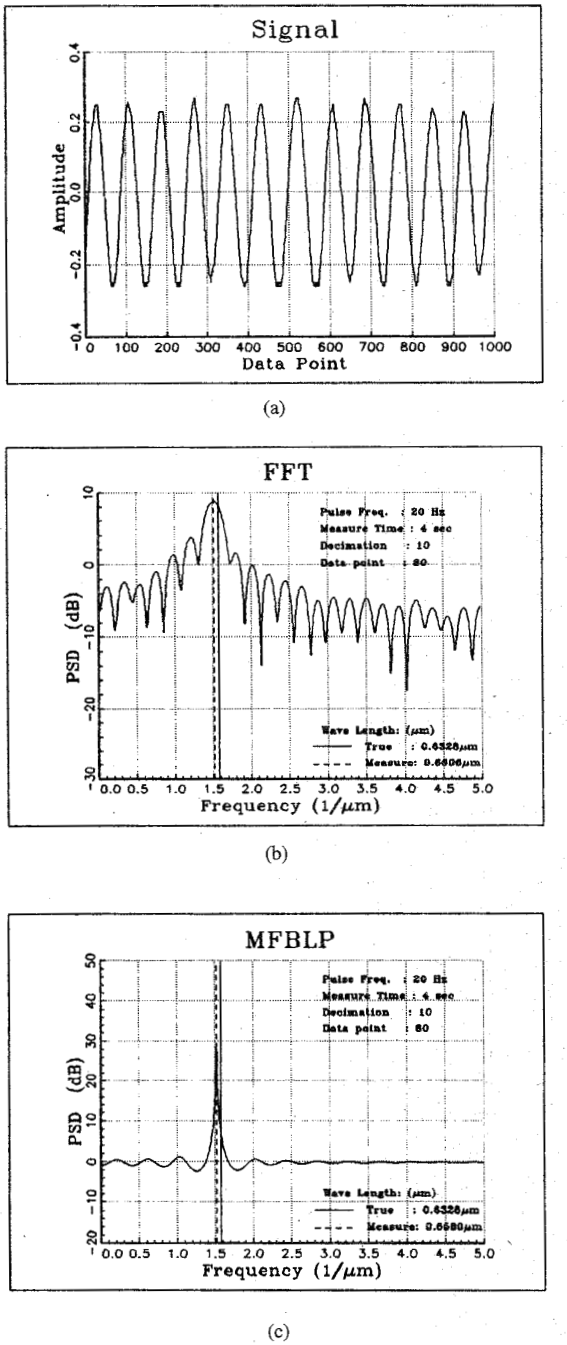

Fig. 10 (a) Waveform of the worst H20-4. (b) FFT of the worst H20-4. (c) MFBLP of the worst H20-4.

is, the FFT with 8,192 points is used. Since we have only 240 data points as in Table II, we need to pad 7,952 zeros to have 8,192 points. The spectral resolution by the previous process is pointed out in Table III, and the result is exactly the same as in Table I. From these three tables, we can conclude that the result of wavelength estimation with $D = 8$ having 60 decimated data points outperformed the one with $D = 2$ having 240 decimated data points.

As we mentioned previously, the frequency of the cosine function is $f = \frac{2v}{\lambda}$. After the sampling process, the corresponding normalized digital frequency f' of f is given by

$$f' = f \cdot T_s \tag{21}$$

where $T_s = t/N$ is the sampling period measured in seconds/data length. Defining the digital frequency, f'', which is the normalized digital frequency multiplied by the decimation factor D, that is, $f'' = f \cdot T_s \cdot D = f' \cdot D$, and substituting $f = \frac{2v}{\lambda}$, T_s and (21) to f'', we have

$$f'' = f' \cdot D = \frac{2v}{\lambda} \cdot \frac{t}{N} \cdot D. \tag{22}$$

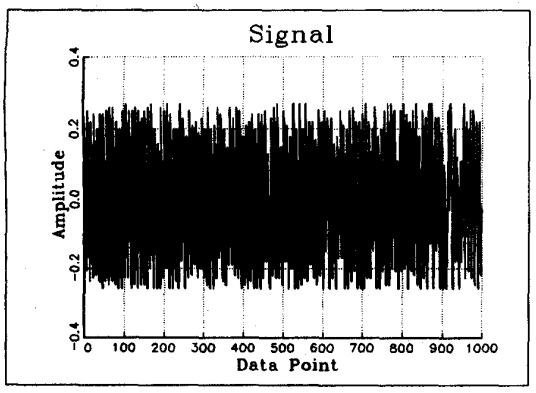

(a)

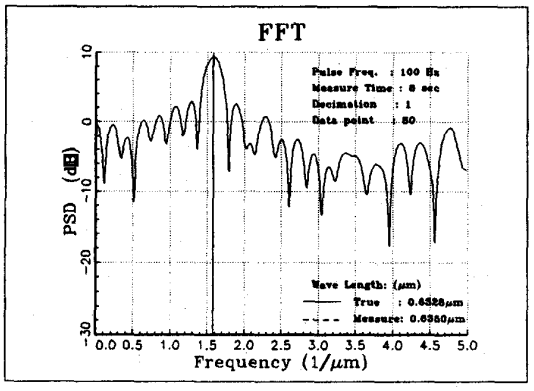

(b)

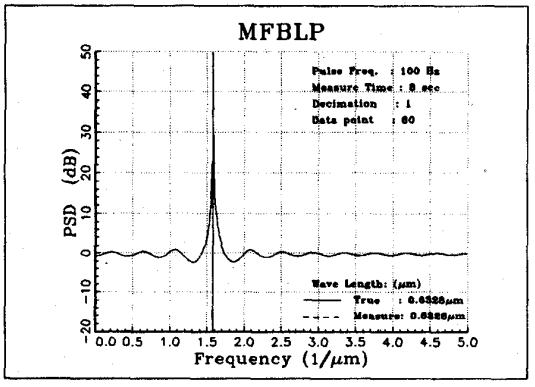

(c)

Fig. 11. (a) Waveform of the H100-8. (b) FFT of the H100-8. (c) MFBLP of the H100-8.

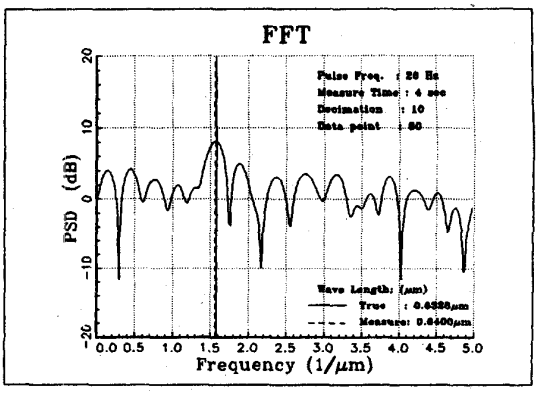

(a)

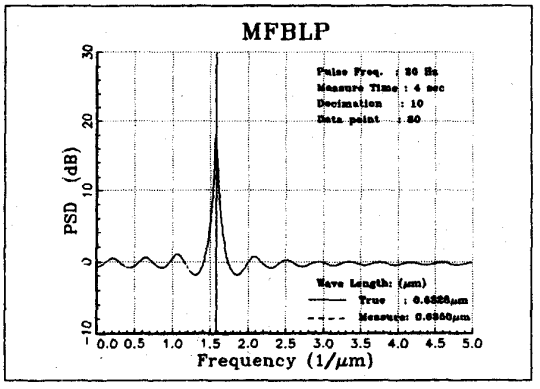

(b)

Fig. 12. (a) FFT in SNR=0 dB. (b) MFBLP in SNR =0 dB.

Since in the sampling process the range of digital frequency should be less than 0.5, the range of digital frequency, f'', should be $0 < f'' < 0.5$. From Tables I and II, we see that the spectral resolution will go from fine to bad if $f'' < 0.1$, because the index 207 in Table I, with $D = 8$, did not have the corresponding index, 51.7, in Table II, with $D = 2$. Instead, the main lobe of the spectrogram in Table II, is at index 52 which is in accordance with the index 208 in Table I. Alternatively, we may say that to have good resolution the range of frequencies, f'', is simply limited by (see Tables I and II)

$$0.1 < f'' < 0.5. \tag{23}$$

Substituting (22) into (23) we get

$$0.1 < \frac{2v}{\lambda} \cdot \frac{t}{N} \cdot D < 0.5. \tag{24}$$

Let the mirror's moving speed, v, be a parameter; by definition, we have

$$v = \frac{\text{pulse number}}{\text{second}} \times \frac{\text{unit distance}}{\text{pulse}} = \frac{\text{translate distance}}{\text{second}}$$

where

$$\frac{\text{pulse number}}{\text{second}} = \text{frequency sent out by pulse generator}$$

and

$$\frac{\text{unit distance}}{\text{pulse}} = \text{minimum distance traveled by translator.}$$

Since $2v$, equal to the pulse generator frequency (f_p) multiplied by 0.1 μm, the wavelength, equal to 0.6328 μm,

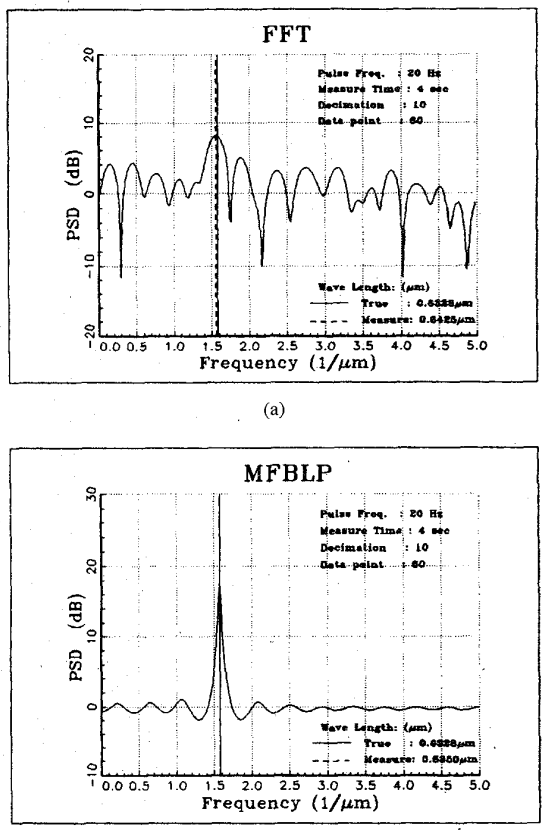

Fig. 13. (a) FFT in SNR $= -3.0$ dB. (b) MFBLP in SNR $= -3.0$ dB.

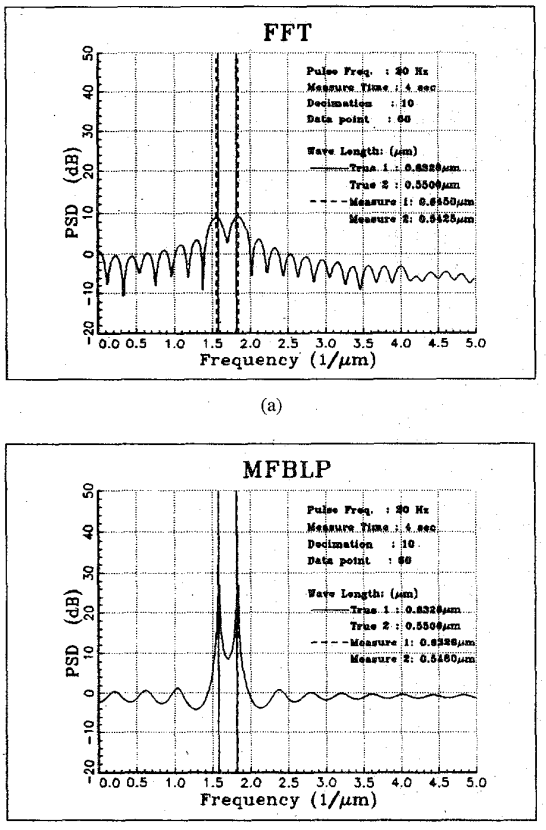

Fig. 14. (a) FFT method. (b) MFBLP method.

$N = 1000$, and D, the decimation factor, are all known, substituting these into (24), we have

$$632 < f_p \cdot t \cdot D < 3164 \tag{25}$$

where f_p represents the value of the pulse generator frequency in Hz units.

As mentioned in [3], the sampling rate depends on the spectral range of the material. Through the above discussion, we also found that the spectral resolution is not only affected by the data length, but also significantly affected by the decimation factor. Consequently, if a fairly good result is to be obtained, the conditions of (24) or (25) must be satisfied.

On the other hand, the spectrogram of the optical signal using the MFBLP method with search algorithm is evaluated by $S(\omega)$ in (18). Since $S(\omega)$ is a continuous function of ω, we can enhance the spectral resolution in the following way: When the spectrogram is obtained, we divide the scale of the frequency axis into a more precise scale in the vicinity of the main lobe peak. Through the above processing, the spectral resolution can then be enhanced because the estimated values have more precision corresponding to the new frequency scale. However, the frequency scale corresponding to the FFT algorithm is limited by the data length, such that the resolution can not be improved. Moreover, the search algorithm developed is a new method, which automatically extracts the principal eigenvalues corresponding to the different optical wavenumbers, and a good result can be obtained. Therefore, the MFBLP method can achieve a good result in practice when the search algorithm is employed.

Finally, to further compare the result of the FFT method with the method of MFBLP along with the search algorithm in the noisy case, we induced additive white noise, which is produced by the computer, into the optical signal H20-4. After computer simulation, Figs. 12 and 13 show the results for the signal-to-noise ratio in 0 dB and -3 dB, respectively. Since the signal waveform has been distorted by the induced noise, the FFT method can not obtain satisfactory results. Conversely, the MFBLP method with search algorithm can obtain the desired result and has a strong tolerance in the noisy case compared to the FFT method.

Moreover, as described earlier in this section, to reduce the computational effort for evaluating the spectrogram using the MFBLP method, the length of data points and the number of tap weights have to be decreased. Table IV shows the computational requirements and the results of wavelength estimation related to the length of data points and the tap weight number. The average computation time for evaluating the spectrogram using the FFT method with 2048 points is 0.1245 s. However, from Table IV, we can see that satisfactory results can still be achieved for the MFBLP method with $D = 10$, for 40 data points and 10 tap weights. The computation

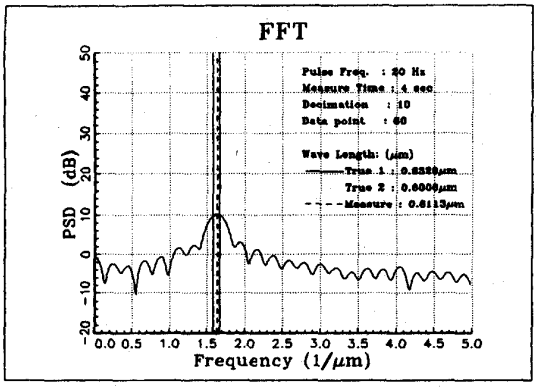

(a)

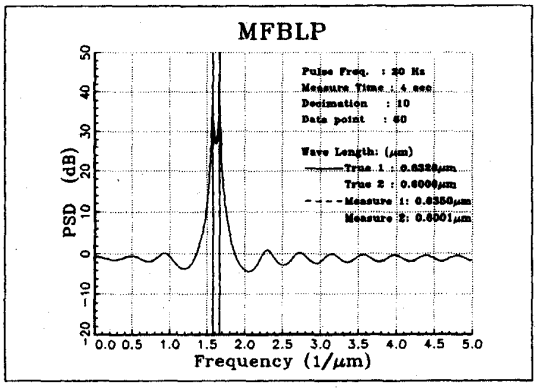

(b)

Fig. 15. (a) FFT method. (b) MFBLP method.

time in this case is 0.0441 s, which is much less than the one using the FFT method.

IV. Conclusion

In this paper, we have shown that the merits of the MFBLP method are truly greater than those of the conventional FFT. In practice, since the number of principal eigenvalues is not known in advance, the search algorithm will be useful and can achieve the desired results for the wavelength estimation. Problems such as sampling rate, data length and the effect due to the decimation factor have also been discussed. From experimental results, we conclude that to have the desired result using the FFT method the condition, $632 < f_p \cdot t \cdot D < 3164$, has to be satisfied. Due to budget and equipment limitations, we could not use the proposed method for multiple-wavenumber measurement. However, to document the advantage of the method presented, a computer simulation for two-wavenumber estimation is investigated. For this purpose, we induced the additive signal with wavelength $\lambda_2 = 0.6000$ μm or $\lambda_2 = 0.5500$ μm, which is produced by the computer, into the optical signal set, H20-4. From the simulation results of Figs. 14(a) to 15(b), we nevertheless believe that the proposed method is superior to the FFT method and can be successfully applied to other problems of spectrum analysis.

References

[1] M. Francon, Ed., *Optical Interferometry*. New York: Academic, 1984, pp. 87–96.
[2] R. J. Bell, Ed., *Introductory Fourier Transform Spectroscopy*. New York, San Francisco, London: Academic, 1972, p. 33.
[3] Y. P. Lee, "Introduction to Fourier transform infrared spectrometer (FT-IR)," *Instruments Today*, vol. 4, no. 2, pp. 29–37, 1983.
[4] D. W. Tufts and R. Kumaresan, "Estimation of frequencies of multiple sinusoids: Making linear prediction perform like maximum likelihood," *Proc. IEEE.*, vol. 70, no. 9, pp. 975–989, 1982.
[5] S. Haykin, Ed. *Adaptive Filter Theory*. Englewood Cliffs, NJ: Prentice-Hall Inc., pp. 122–188, 1986.
[6] S. M. Kay, *Modern Spectral Estimation: Theory and Application*. Englewood Cliffs, NJ: Prentice-Hall, 1988.
[7] L. J. Griffiths, "Rapid measurement of digital instantaneous frequency," *IEEE Trans. Acoust., Speech, Signal Processing*, vol. ASSP-23, no. 2, pp. 207–222, 1975.
[8] S. J. Chern and K. M. Wong, "Recirculation of input data in frequency-domain adaptive filtering," *The Canadian Elec. Eng. Journal*, vol. 12, no. 3, pp. 90–98, 1987.
[9] A. V. Oppenheim, *Discrete-Time Signal Processing*. Englewood Cliffs, NJ: Prentice-Hall, 1991, pp. 105, 111, 127–129.
[10] R. E. Crochiere and L. R. Rabiner, *Multirate Digital Signal Processing*. Englewood Cliffs, NJ: Prentice-Hall, 1983.

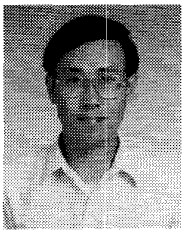

Shiunn-Jang Chern received the B.S. degree from Tamkang University, Taipei, Taiwan, R.O.C., in 1977, the M.S. degree from the Southeastern Massachusetts University, North Dartmouth, in 1982, and the Ph.D. degree from the McMaster University, Hamilton, Ontario, Canada, in 1986.

He is currently a Professor in the Electrical Engineering Department at National Sun Yat-Sen University, Kaohsiung, Taiwan, R.O.C. His research interests include statistical analysis of an adaptive filtering algorithm, time-delay estimation, optical signal processing, and array signal processing.

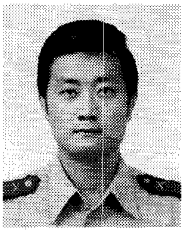

Kuo-Jiann Chao was born in Taiwan on December 4, 1957. He received the B.S. degree in physics from Chinese Military Academy, Fengshan, Taiwan, in 1980, and the M.S. degree in applied physics from Chung Cheng Institute of Technology, Taoyuan, Taiwan, in 1987.

Since September 1990, he has been working as a Research Assistant and is also a full-time graduate student working towards the Ph.D. degree in electrical engineering at the National Sun Yat-Sen University, Kaohsiung, Taiwan. His research interests include optical signal processing and microwave images.